PCCP

PAPER

View Article Online
View Journal | View Issue

Cite this: *Phys. Chem. Chem. Phys.*, 2016, **18**, 20312

Step dynamics and oxide formation during CO oxidation over a vicinal Pd surface

Mikhail Shipilin,* Johan Gustafson, Chu Zhang, Lindsay Richard Merte and Edvin Lundgren

Received 4th December 2015,
Accepted 20th January 2016

DOI: 10.1039/c5cp07488f

www.rsc.org/pccp

In an attempt to bridge the material and pressure gaps – two major challenges for an atomic scale understanding of heterogeneous catalysis – we employed high-energy surface X-ray diffraction as a tool to study the Pd(553) surface *in situ* under changing reaction conditions during CO oxidation. The diffraction patterns recorded under CO rich reaction conditions are characteristic for the metallic state of the surface. In an environment with low excess of O_2 over the reaction stoichiometry, the surface seems to accommodate oxygen atoms along the steps forming one or several subsequent adsorbate structures and rapidly transforms into a combination of (332), (111) and (331) facets likely providing the room for the formation of a surface oxide. For the case of large excess of O_2, the diffraction data show the presence of a multilayer PdO with the [101] crystallographic direction parallel to the [111] and the [331] directions of the substrate. The reconstructions in O_2 excess are to a large extent similar to those previously reported for pure O_2 exposures by Westerström *et al.* [R. Westerström *et al.*, *Phys. Rev. B: Condens. Matter Mater. Phys.*, 2007, **76**, 155410].

1 Introduction

Many industrial and everyday processes surrounding us result in the production of poisonous substances. One of the most common cases is the emission of CO gas – a highly toxic pollutant, which heavily affects the environment and human health – by *e.g.* fuel combustion engines. The well-established way to remove this unwanted product is utilization of catalytic converters that allow for oxidation of CO to $CO_2\left(CO + \frac{1}{2}O_2 \rightarrow CO_2\right)$ – a process which cannot proceed efficiently in the gas phase under regular conditions and requires the presence of a catalyst.[1–4]

Modern catalysts consist of a porous substrate supporting nanoparticles of a certain composition active towards particular chemical reactions. It allows for a drastically increased efficiency through maximization of the active area per unit of volume. However the complex structure of the catalysts prevents application of most experimental methods of surface characterization. Another difficulty arises due to inability of many surface sensitive experimental techniques to operate under realistic conditions, especially high pressure. Thus, in order to develop new catalysts and improve existing ones, simplified model systems such as single crystals are studied under UHV conditions. The inconsistency between real and model catalysts is referred to as material and pressure gaps.

Pd metal is a highly efficient catalyst for CO oxidation.[5] The Pd(553) crystal studied in this work exposes undercoordinated step-atoms, which to a certain extent can simulate the behavior of the atoms on the edges of nanoparticles in a real catalyst.[6–10] High-energy surface X-ray diffraction allows us to follow the processes occurring on the surface of a model catalyst under realistic conditions due to the high penetration ability of utilized radiation.[11–13] Thus, the results of the studies of the chosen system with this particular experimental tool allow us to obtain new information, which potentially could help to bridge the pressure gap and to a certain extent the material gap.

Oxidation of the Pd(553) surface in pure oxygen was thoroughly studied over a broad pressure range by Westerström *et al.* using several *in situ* and *ex situ* experimental techniques and *ab initio* simulations.[14] The authors showed that with increasing pressure the surface undergoes several oxygen induced transformations. They also notice that studies of the structural changes in this catalytic system under real working conditions would be of great importance for the comprehension of heterogeneous catalysis.

This idea motivated us to study the Pd(553) surface acting as a catalyst in the process of CO oxidation and to compare our results with the results obtained by Westerström *et al.* for the surface exposed to pure oxygen. For that purpose in the following work we employ high-energy surface X-ray diffraction. We change the gas composition in the reactor from CO rich to O_2 rich relatively to the stoichiometric reaction ratio while recording the diffraction data *in situ*. The results show that the surface structure drastically changes sequentially adopting several states upon the catalyst activation and providing a room for the thick PdO film growth when the O_2 excess is significant.

Division of Synchrotron Radiation Research, Lund University, SE-22100 Lund, Sweden. E-mail: mikhail.shipilin@sljus.lu.se; Tel: +46 (0) 46 222 04 69

2 Experimental details

A Pd(553) single crystal was placed in an ultra-high vacuum (UHV) chamber combined with a gas flow reactor.[15] This setup allowed us to employ standard surface science sample preparation tools and to expose the sample to a gas mixture at total pressures of up to 1 bar in the separate volume of 50 ml accessible to X-rays through a Be dome. Flows of Ar, CO and O_2 gases were controlled individually by mass-flow controllers and mixed before entering the reactor. An active carbonyl trap insured the absence of metal carbonyls in the gas feed. The partial pressures of the reactants and the reaction products were continuously followed with a quadrupole mass spectrometer using a controlled leak from the reactor volume to the UHV part of the chamber.

The experiments were done in experimental hutch 2 at beamline P07 at PETRA III, Deutsches Elektronen-Synchrotron (DESY) in Hamburg, Germany. X-ray radiation with an energy of 85 keV and photon flux on the order of 5×10^{10} photons per s was employed. The surface of the sample was precisely aligned at an incident angle of 0.04° using a HUBER diffractometer.[16] The angle of incidence was chosen close to the critical angle of total external reflection for palladium in order to maximize the diffraction signal from the surface.

Prior to the measurements the sample was cleaned by cycles of Ar^+ sputtering at 1.5 keV and annealing up to 1000 K. This procedure was repeated several times until the diffraction pattern characteristic for Pd(553) surface was observed, see below. The clean sample was heated to 600 K and kept at that temperature throughout the entire experiment. The crystal was exposed to the gas mixture at the total pressure of 100 mbar in the flow rector. The composition of the gas feed could be promptly changed in order to change reaction conditions.

The gas feed consisted of CO, and O_2 for the reaction, while Ar was acting as a carrier gas. The flow of CO was set to the constant rate of 4 $ml_n\ min^{-1}$ (1 $ml_n\ min^{-1}$ corresponds to 1 ml min^{-1} at 0 °C and 1013 mbar) while the flows of O_2 and Ar were changed relatively to each other in order to increase or decrease the ratio between CO and O_2 while keeping the total gas flow constant at 50 $ml_n\ min^{-1}$. This allowed us to change the gas composition in the reactor while maintaining the constant pressure of 100 mbar. Three different O_2/CO gas ratios were used in the experiment, namely $\frac{1}{4}$ (2 mbar O_2, 8 mbar CO partial pressure), $\frac{2.1}{4}$ (4.2 mbar O_2, 8 mbar CO) and $\frac{1}{1}$ (8 mbar O_2, 8 mbar CO).

To describe the crystal structure of Pd(553) surface a monoclinic basis set of vectors $\mathbf{a}_1 = \left(-\frac{1}{2}a_0,\ \frac{1}{2}a_0,\ 0\right)$, $\mathbf{a}_2 = \left(-\frac{3}{2}a_0,\ 0,\ \frac{5}{2}a_0\right)$ lying in the surface plane under the angle of 111.3° to each other and $\mathbf{a}_3 = (5a_0,\ 5a_0,\ 3a_0)$ perpendicular to them was used (a_0(Pd) = 3.89 Å is the bulk lattice constant of Pd). The lengths of these vectors are 2.75, 11.34 and 29.88 Å respectively. The corresponding lengths of reciprocal lattice basis vectors are thus 2.45, 0.60 and 0.21 $Å^{-1}$ and they are referred to as reciprocal lattice units (RLU) throughout the work.

The schematic diagram of the experimental setup is shown in Fig. 1. Scattered photons were collected by a 410 × 410 mm^2 Perkin-Elmer flat panel X-ray detector with a 4-megapixel resolution specially designed for high-energy radiation. The areas

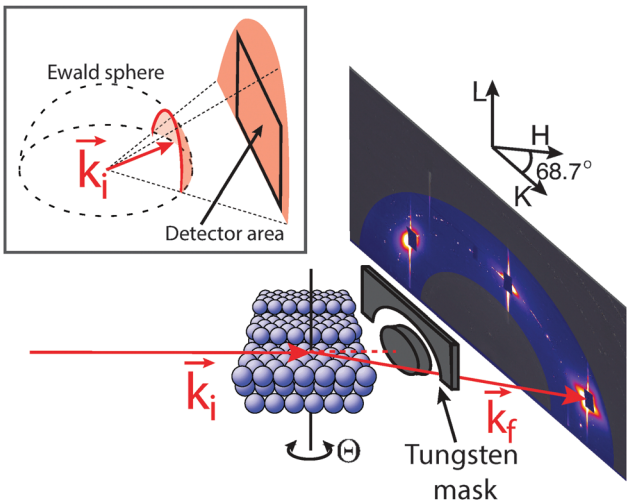

Fig. 1 Schematic diagram of the experimental setup. The incident beam hits the sample surface and scattered photons are collected with an area detector. The direct beam and undesired scattering from the reactor walls are suppressed by the tungsten mask causing shading of certain parts of the images (shown with gray color in the image). Intense Bragg peaks are also covered to protect the detector from oversaturation. The inset in the top left corner shows schematically the part of Ewald sphere that can be visualized by the detector.

of the detector where bulk diffraction maxima were expected to appear were covered with Densimet® pieces, which absorb the high intensity radiation that otherwise would cause oversaturation of the sensitive detector elements. This protection results in black rectangular areas in the images. The circular areas on the detector shown in grey color in Fig. 1 are shadowed by the beamstop, which absorbs the direct beam, and the mask, which suppresses the radiation scattered by the walls of the reactor dome made of Be. These shaded areas were excluded from the analysis.

In a diffraction experiment one can potentially observe all points of reciprocal space that lie on the surface of a sphere with the radius proportional to the energy of an incoming radiation, known as the Ewald sphere. In the present experiment, with the detector positioned at the distance of 1750 cm from the sample, it was possible to observe the projection of the part of such a sphere which spans over the area from −5 to 5 $Å^{-1}$ and from 0 to 5 $Å^{-1}$ in in-plane and out-of-plane directions, respectively. The recorded images thus can be imagined to be curved vertical cuts through the reciprocal lattice of the structure under the study. The sample then can be rotated under the incoming beam and the corresponding diffraction patterns can be continuously recorded. This results in a set of images representing the vertical slices of the reciprocal space at different azimuthal angles. After certain post-corrections and processing[12] the three dimensional reciprocal lattice can be restored revealing the periodicity of the structure currently present on the surface.

3 Results and discussion

In our experiment we performed two types of measurements. The first type we refer to as rocking scan analogously to the notion in conventional surface X-ray diffraction. It essentially

involves recording the three-dimensional part of reciprocal space (its approximate projection on the *hk*-plane is shown with the light red color in Fig. 2a), which in this case spanned over 31.2° with the central position coinciding with the *k*-axis of Pd(553) reciprocal lattice and corresponding to the in-plane direction perpendicular to the surface steps in real space (designated as *Y* in Fig. 2b). In this way we were able to observe the step periodicity and the orientation of the facets on the surface of the crystal under different fixed conditions for CO oxidation reaction taking place in the reactor. The second type of measurements was performed at a fixed angular position of the sample where the distinguishing features of the reciprocal lattice could be observed. This type of scan reveals a time resolved dynamics of the diffraction features caused by changes in the reaction environment. In the current work the rotational position of the sample was chosen in a way that the Ewald sphere intersects the *kl*-plane of the reciprocal lattice across a wide range in *k*. The recorded patterns thus allow for qualitative analysis of the surface structure in the direction perpendicular to the surface steps in real space.

3.1 Stationary conditions

For the rocking scans images were recorded every 0.2° of the sample rotation with 1 s exposure time resulting in 156 images in every set. They show the intersection area between Ewald sphere and the reciprocal lattice at the adjacent angles of the sample rotation. It is possible to take the most intense pixels of the images over the whole rocking scan in order to get a two dimensional representation of the recorded part of reciprocal lattice, which in this case displays the actual *kl*-plane of the reciprocal lattice. For Pd(553) metallic surface after cleaning in vacuum the diffraction pattern is shown in Fig. 2d, while Fig. 2c shows a schematic view of *kl*-plane expected for this system (the light red shaded area indicates the region accessible for analysis due to the presence of the mask and the beamstop).

The diffraction pattern of the clean sample contains sharp crystal truncation rods originating from the bulk Bragg maxima at the integer *h*-, *k*-values. This fact indicates that the surface after cleaning has the well ordered structure characteristic for Pd(553) without major imperfections, *i.e.* four atom wide (111)-oriented terraces separated by (11−1)-oriented monoatomic steps.

In Fig. 3a–c three diffraction patterns obtained *via* rocking scans are shown. For clarity, only the right halves of the original diffraction patterns are shown since this region shows features from all relevant structures. The diffraction patterns correspond to the Pd(553) exposed to mixtures of CO and O_2 carried in Ar at 100 mbar total pressure and 600 K temperature (a) with a large excess of $CO(O_2/CO = \frac{1}{4})$, (b) with a small excess of $O_2(O_2/CO = \frac{2.1}{4})$ and (c) with a large excess of $O_2(O_2/CO = \frac{1}{1})$ over the reaction stoichiometry.

The pattern shown in panel (a) appears similar to that of the clean Pd(553) surface in vacuum (see Fig. 2d). Crystal truncation rods (CTRs) are clearly visible and originate from the bulk Pd Bragg maxima with the periodicity characteristic for the well ordered metallic (553) oriented surface. Under these conditions

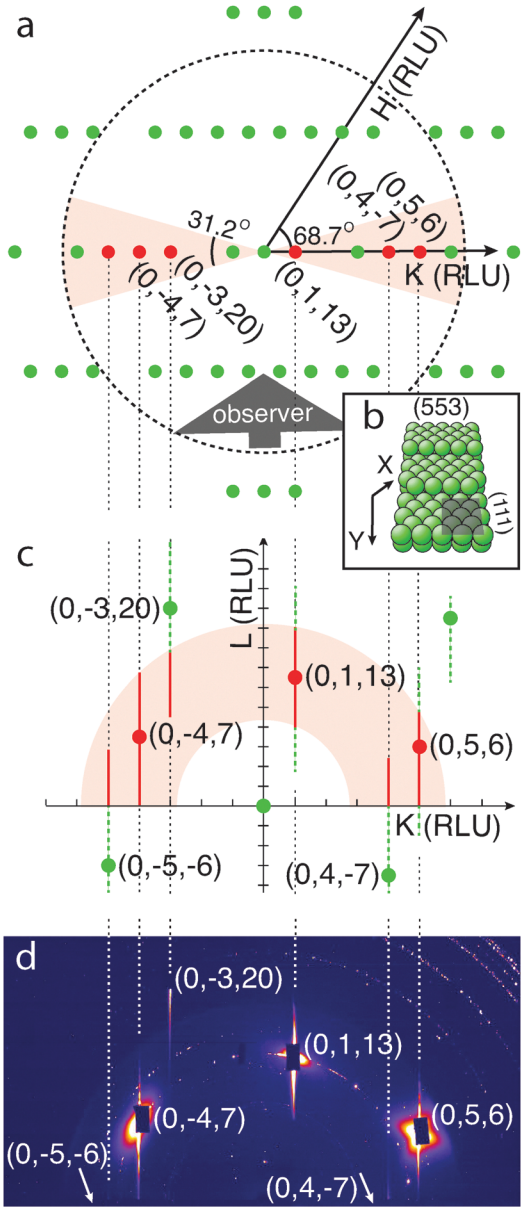

Fig. 2 (a) Schematic view of the projection of the part of the Pd(553) reciprocal lattice on the *hk*-plane. Light red area indicates the volume covered by rocking scans. Bright red circles represent Bragg maxima with corresponding diffraction rods, which are accessible for observation in the experiment. (b) Ball model of Pd(553) surface. (c) Schematic view of the *kl*-plane of Pd(553) reciprocal lattice. The light red area indicates the region accessible for analysis due to the presence of the mask and the beamstop. (d) 2D diffraction pattern representing the *kl*-plane in reciprocal space obtained by integration of a rocking scan performed after cleaning in vacuum.

we assume the surface to be CO poisoned, which means that the reaction is inhibited by CO molecules covering the surface and hindering dissociative adsorption of O_2 species – the behavior observed before for different transition metal surfaces.[17–22] Our mass-spectrometer readings recorded at the same time indeed show only a very low CO_2 production. This can be seen in the mass-spectrometer signal shown in the top right panel of Fig. 4. Although this particular signal corresponds to the time resolved scan,

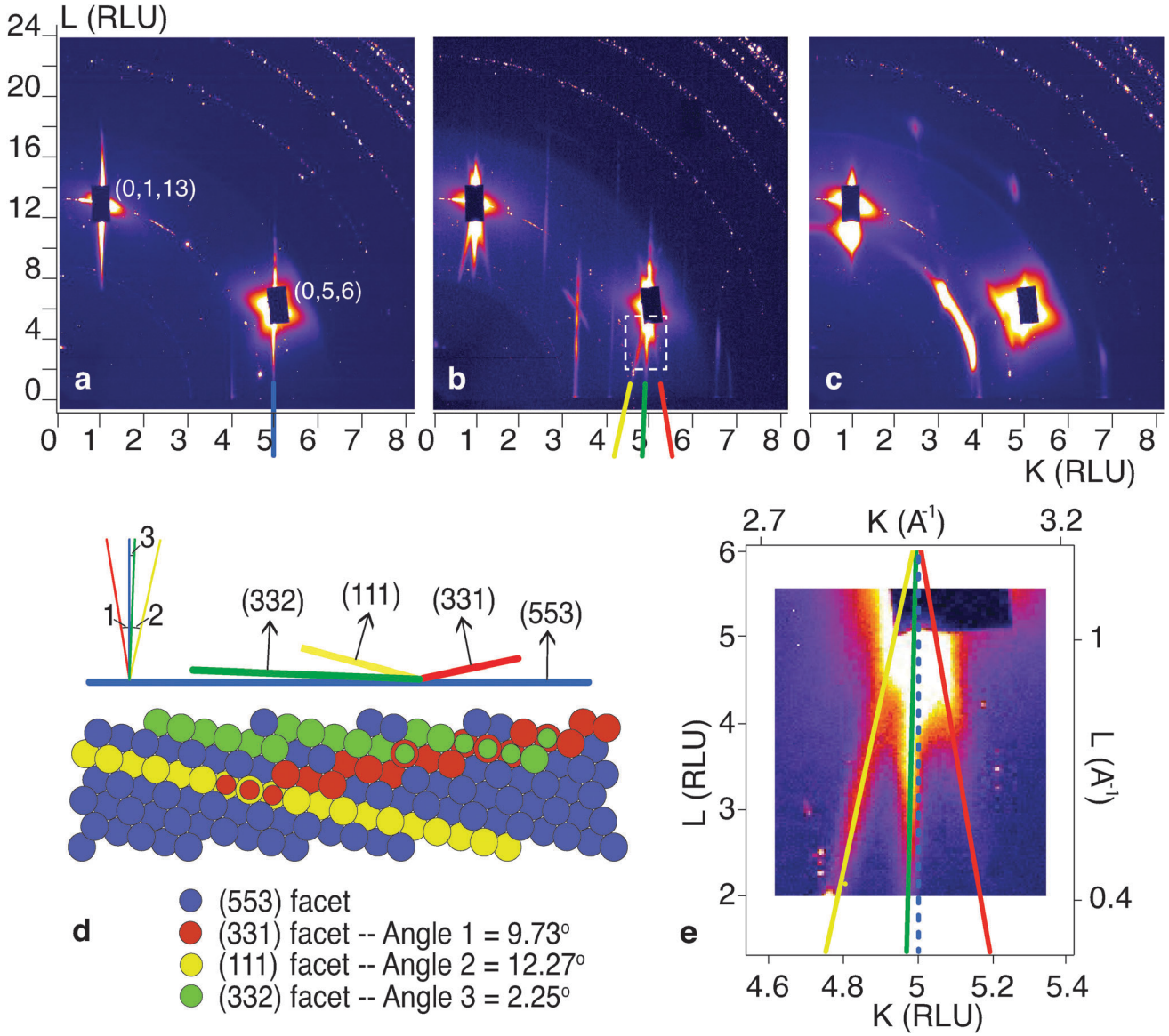

Fig. 3 (a–c) Diffraction patterns from Pd(553) during exposure to mixtures of CO and O_2 carried in Ar at 100 mbar total pressure and 600 K temperature (a) with a large excess of $CO\left(O_2/CO = \frac{1}{4}\right)$, (b) with a small excess of $O_2\left(O_2/CO = \frac{2.1}{4}\right)$ and (c) with a large excess of $O_2\left(O_2/CO = \frac{1}{1}\right)$. (d) Side view of the Pd(553) surface (blue discs) with (332), (111), (331) facets marked with green, yellow and red discs respectively. Overall orientations of these facets and their normals are shown in the same colors. The corresponding angles are given. (e) Magnified area marked with the white dashed rectangle in the panel (b) showing the orientation of the diffraction rods.

which will be discussed later, it is reproducible and shows the same behavior for different scans under the same conditions.

Upon switching to the gas composition with the low excess of $O_2\left(O_2/CO = \frac{2.1}{4}\right)$, the diffraction pattern shows the clear signature of surface restructuring (see Fig. 3b). The vertical CTRs are no longer visible in the diffraction pattern: instead new rods are observed which are tilted at different angles in respect to the surface of the crystal. This behavior is clear evidence of crystal surface refaceting since CTRs are always perpendicular to the surface of their origin. Such surface restructuring was previously reported for different stepped surfaces upon oxidation in pure oxygen[23–25] and for the case of catalytic CO oxidation.[26]

The angular values of CTRs tilt, which can be measured directly from the recorded data, allow us to assign these diffraction features to certain crystallographic planes. In Fig. 3e the magnified area of the diffraction pattern marked with a dashed rectangle in Fig. 3b is shown. The angles between the (553) surface normal and the observed CTRs are 2.05°, 9.88° and 12.28°, which are in a good correspondence with calculated values of 2.25°, 9.73° and 12.27° for (332), (331) and (111) crystallographic planes respectively. Additionally, in Fig. 3b one can see several parallel diffraction rods corresponding to the (332) crystallographic orientation separated by a distance smaller than between the original (553)-oriented CTRs. It indicates that the average step periodicity of the corresponding

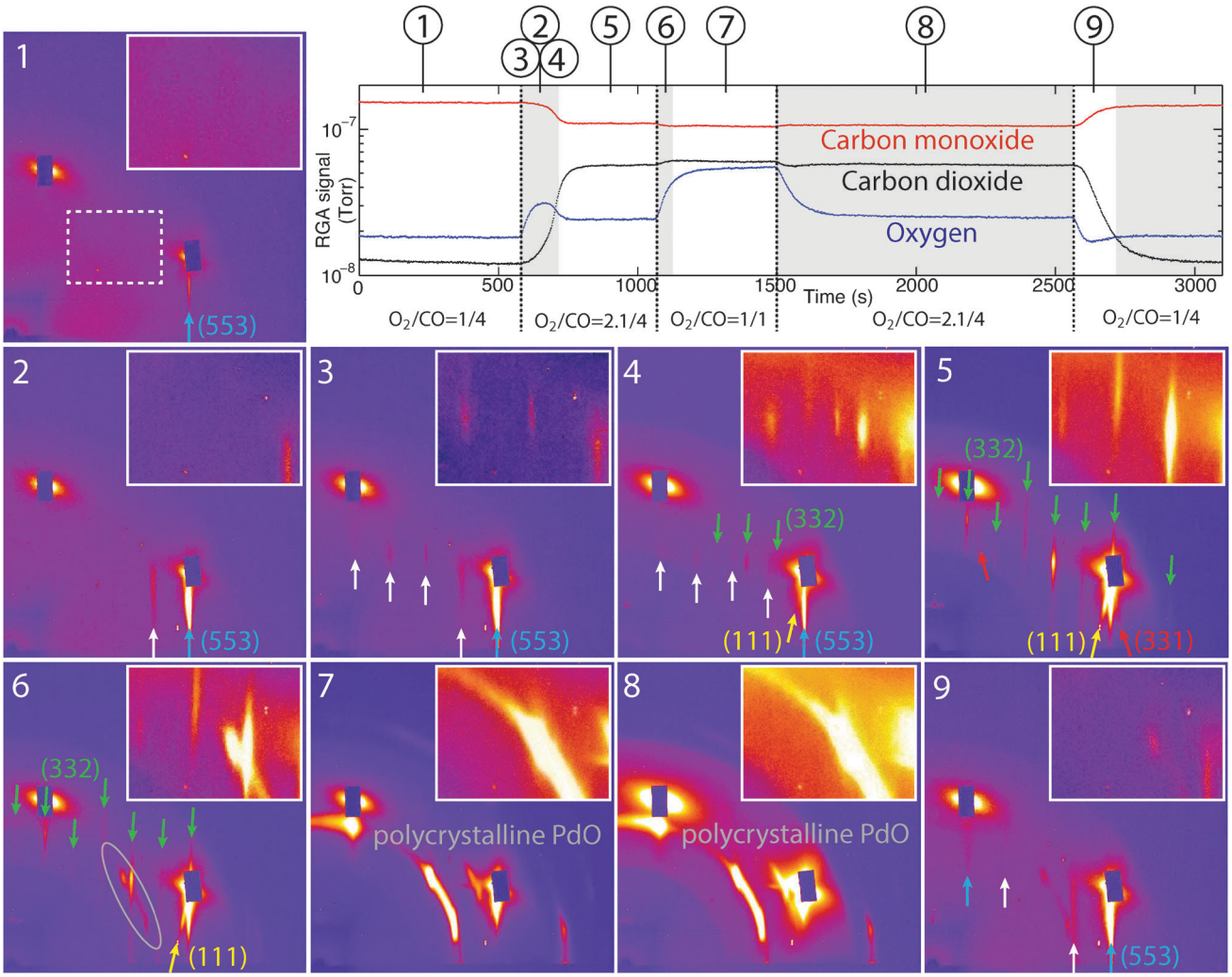

Fig. 4 Mass-spectrometer readings (top-right corner) with the marked time intervals when the corresponding diffraction patterns (panels 1–9) were recorded. The insets in the top-right corner of each panel show the magnified region indicated by the dashed rectangle in the panel 1.

facets has changed towards slightly wider terraces. This change precisely corresponds to the periodicity of Pd(332) surface, which contains five atoms wide (111)-oriented terraces separated by (11−1)-oriented monoatomic steps with a periodicity of 12.9 Å.

In their work Westerström *et al.* observed a similar type of Pd(553) surface refaceting in pure oxygen.[14] Based on a large set of data collected using several experimental techniques and theoretical calculations, the authors concluded that upon oxidation the majority of the surface rearranges into areas with (332) crystallographic orientation alternated by (111), (110), (221) and (775) facets, which naturally form in order to maintain the overall (553) orientation of the crystal surface. The suggested reason for this refaceting is the growth of a PdO(101) surface oxide structure, which fits on the (332)-oriented surface because its terrace width is similar to the size of the unit cell of the surface oxide.

In our experiment, under reaction conditions for CO oxidation, we also see the surface refaceting, although different. The formation of (332), (331) and (111)-oriented facets is observed. We don't see any fingerprints of (110), (221) and (775) facets, however, it may be due to their low concentration on the surface, which was the case for (221) and (775) facets formation in pure oxygen. On the other hand we observe the formation of (331)-oriented facets, which were not found by Westerström *et al.* It in principal can be explained by the fact that (110)- and (331)-oriented facets can perform the similar role, namely compensate the (332)-oriented facets for overall surface correction to keep the initial (553) orientation.

At the same time with the surface refaceting the mass-spectrometry data (see the top right panel of Fig. 4) show the production of CO_2 at a high level limited by the rate of gaseous CO transport to the surface (often referred to as the mass transfer limit). The catalytic activation of the sample together with the discussed simultaneous surface refaceting suggests the likely formation of a surface palladium oxide with (101) crystallographic orientation covering the terraces of the newly formed (332) facets. Such conclusion can be made based on the fact that, first, surface PdO in different structural variations including the (101) was found in many cases to be the active

phase of Pd model catalysts for the reaction of CO oxidation[5,12,22,27] and, second, the formation of surface PdO(101) would be in agreement with the results obtained by Westerström *et al.* and would explain the domination of (332) facets on the surface, since the terraces there have a size suitable for accommodation of the (101) plane of the PdO unit cell.

After switching the gas composition to the relatively large excess of O_2 ($O_2/CO = \frac{1}{1}$), the diffraction pattern drastically changes (see Fig. 3c) while the mass-spectrometry data (see the top right panel of Fig. 4) do not show a significant difference in CO_2 production. The catalytic activity of the sample under these conditions is mass-transfer limited. At the same time the elevated oxygen partial pressure over the surface leads to the growth of bulk PdO, which is indicated by the disappearance of CTRs and presence of diffuse spots of enhanced intensity and parts of diffraction rings with the positions characteristic for PdO. Such pattern indicate a preferential orientation of growth of the bulk oxide. The positions of the maxima can be well explained by the growth of a multilayer PdO with the [101] crystallographic direction parallel to the [111] (yellow diamonds in Fig. 5 shows expected positions for this orientation of the film) and the [331] (red circles Fig. 5) directions of the substrate. The step distance between edge atoms on the (331) facets is about 6 Å which can potentially accommodate the (101) crystallographic plane in the PdO unit cell with 6.14 Å size of the long side. At the same time it was shown that a (111)-oriented Pd surface provides room for the two dimensional Pd_5O_4 growth[28] followed by a multilayer PdO(101) formation.[29,30] Besides, the PdO(101) multilayer on Pd(111) was experimentally and theoretically found to be catalytically active towards the reaction of CO oxidation[31–34] which is in agreement with the catalytic activity that we observe in our experiment under the oxygen rich conditions. The observed growth of a multilayer PdO with the [101] crystallographic direction parallel to the [111] indicates the larger surface rearrangement including the formation of extended (111) oriented facets on the surface.

The suggested structure of the thick PdO layer formed under excess oxygen differs from the results obtained by Westerström *et al.* in high pressures of pure oxygen. They observed namely the formation of thick PdO with (021) crystallographic orientation covering the steps of the surface. It is possible that this difference occurs because of the CO oxidation reaction which proceeds in our case or because of different thickness of the PdO in the two experiments.

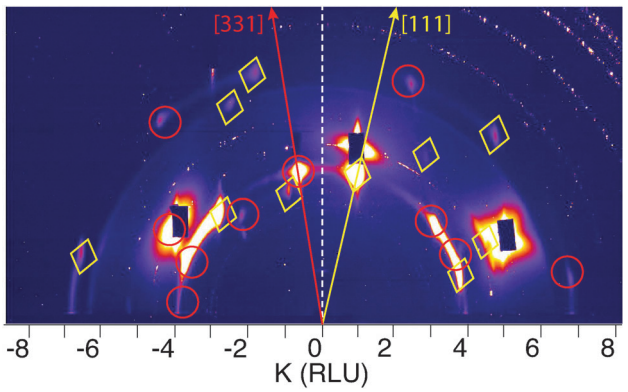

Fig. 5 Diffraction pattern recorded under oxygen rich reaction conditions. Yellow diamonds and red circles indicate the positions of diffraction maxima arising from the multilayer PdO growing with the [101] crystallographic direction parallel to the [111] and the [331] directions of the substrate respectively.

3.2 Dynamic conditions

In order to observe dynamic changes in the surface structure, which may occur on a shorter time scale than accessible by rocking scans, images were recorded at a fixed angular position, as described above. This allowed us to follow surface transformations with one second time resolution during changing reaction conditions. The diffraction patterns were recorded during the exposure of Pd(553) surface to the same mixtures used for the rocking scans, cycling from oxygen-poor to oxygen-rich and back again (see Fig. 4).

In Fig. 4 diffraction patterns are shown along with the mass spectrometer readings. In panels 1–9 it can be seen that the surface indeed adopts more states than observed during the rocking scans. Panels 1, 5 and 8 correspond to the situations reported in Fig. 3a–c, with a metallic surface poisoned with CO molecules, a refaceted surface and a surface covered with bulk PdO, respectively. Other panels in Fig. 4 represent intermediate states of the surface.

Panel 1 in Fig. 4 shows the crystal truncation rod originating from the metallic Pd(553) surface. It is weak but increases in intensity in the subsequent panels. This change in the CTR intensity happens due to the setup alignment, which is very sensitive to the vertical position of the sample surface in relation to the incoming beam. CO oxidation is an exothermic reaction, which releases heat thus causing a thermal expansion of the crystal upon the catalyst activation. Although small, this expansion affects the experimentally recorded data significantly, which results in a loss of intensity in an interference pattern recorded by the detector. In the case of stationary reaction conditions and rocking scans it is possible to correct the alignment before recording data. However, in the case of a continuous scan under changing reaction conditions such correction is not a trivial task. For this reason the sample in the latter case is intentionally slightly misaligned in the beginning of the scan and comes to the desired position upon ignition of the reaction.

When switching from CO rich to O_2 rich reaction conditions, before the complete refaceting, the surface adopts several intermediate states. In panels 2–3 one can see the appearance of additional diffraction rods (marked with white arrows) perpendicular to the (553) surface and with the in-plane periodicity corresponding to the distance between the steps on Pd(553). Such a diffraction pattern would be expected for a two dimensional structure with the same periodicity as the steps of (553) surface. Considering the fact that oxygen partial pressure has increased over the surface, it is logical to suggest that the change in diffraction patterns occurred due to oxygen induced restructuring of the surface.

A number of studies shows that surface step sites play a key role in the adsorption and dissociation of gas molecules.[35–44]

In the case of surface exposure to molecular oxygen, such preference for dissociation sites would result, at least on the initial stages, in decoration of the steps with atomic oxygen. According to theoretical calculations and experimental data obtained by Westerström *et al.* for the case of Pd(553) oxidation in pure oxygen under pressures below 10^{-5} mbar, adsorbed oxygen dissociates and starts to subsequently form three different adsorbate structures along with the pressure increase[14] (see Fig. 6(a–c)). Under such conditions using surface X-ray diffraction the authors observe the appearance of additional diffraction rods at the integer *k*-positions of Pd(553) reciprocal lattice. Our data recorded under reaction conditions exhibit a similar change in diffraction pattern, which can mean that before refaceting the surface of our sample subsequently adopted some or all of the adsorbate oxygen structures found by Westerström *et al.*

In panel 4 of Fig. 4 the diffraction rods assigned to Pd(553) steps with adsorbed oxygen atoms are weaker and coexist with the appearing diffraction rods characteristic for (332) and (111)

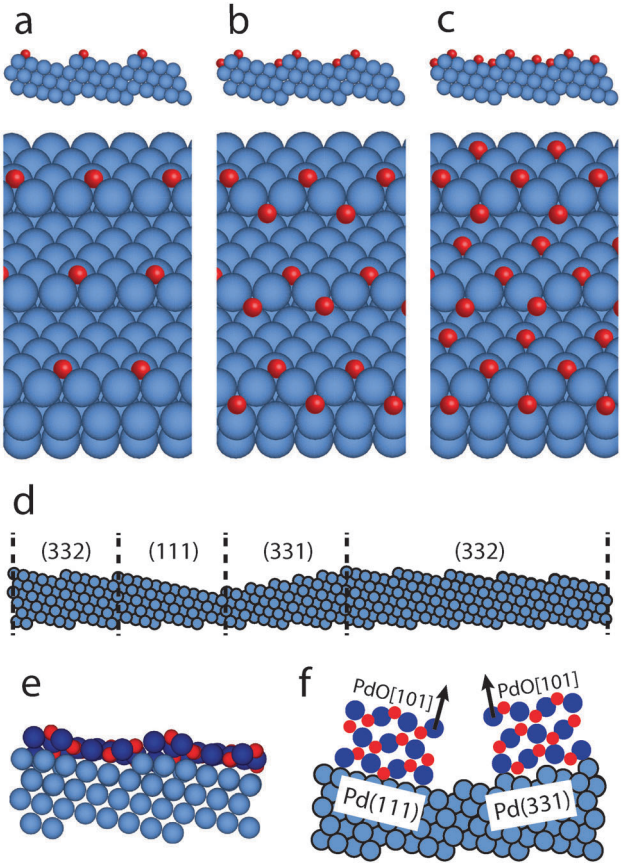

Fig. 6 Schematic ball-models of the surface structure under different conditions. (a–c) Oxygen atoms adsorbed on the steps in different superstructures (models theoretically found by Westerström *et al.* for a Pd(553) single crystal surface exposed to a low oxygen pressure). (d) Refaceting of the (553)-oriented surface into a combination of (332), (111) and (331) facets. (e) Surface PdO covering (332)-oriented facets. (f) Multilayer PdO growing with the [101] crystallographic direction parallel to the [111] and the [331] directions of the substrate. Notice that the size of the O and Pd atoms in the figure is not in line with the corresponding ionic radius for the purpose of visibility.

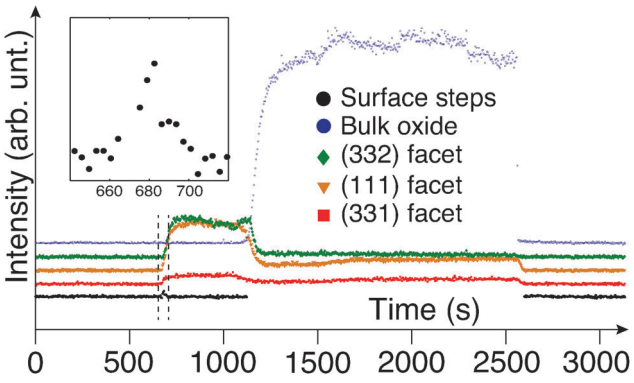

Fig. 7 Intensity of diffraction rods extracted from the data recorded during the continuous scan under changing reaction conditions (the same data set as shown in Fig. 4). The inset clearly shows the appearance of diffraction rods assigned to oxidized steps.

facets indicating the surface transition state before the complete transformation to a combination of (332), (111) and (331) facets represented by the diffraction pattern in panel 5. Panel 6 shows the surface transition to the state when it is fully covered with the bulk PdO (panels 7 and 8). Diffused elongated diffraction maxima appear in the image showing that the oxide grows, at least in the beginning, with a certain degree of preferential orientation dictated by the surface. At the same time, first (331) rods, and then all CTRs disappear, showing that the surface becomes rough. Panel 9 shows the pattern recorded for the surface before it comes back to the initial metallic (553) state upon reducing the oxygen partial pressure. It can be seen that before the complete recovery, the surface produces a weak signal coming from the steps and from the remaining bulk PdO. A further improvement in the time resolution of the employed experimental technique would probably help to resolve the intermediate surface restructuring upon recovery.

In Fig. 7 the extracted intensity of different diffraction features is shown as a function of time. It corresponds to the continuous scan presented in Fig. 4. The inset in Fig. 7 shows the increase of intensity corresponding to the diffraction rods assigned to oxygen adsorbate structures. One can see that the period of existence for the oxygen induced superstructures on the initial stage is about 30 seconds.

4 Conclusions

Under CO oxidation reaction conditions the surface of Pd(553) crystal undergoes several structural changes. In the gas mixture rich with CO the surface is metallic, while the catalytic activity is suppressed by CO molecules covering the surface. Upon increase of the oxygen partial pressure, the observed changes in the diffraction pattern indicate a mild surface restructuring caused most likely by oxygen atoms adsorbed on the steps (see Fig. 6(a–c)). At the same time the catalytic production of CO_2 starts to increase rapidly and reaches the maximum rate limited by the confined transport of gaseous CO to the surface when the composition of the gas mixture entering the reactor stabilizes at the ratio $O_2/CO = \frac{2.1}{4}$. Diffraction data show that

the (553) crystal surface reconstructs into a combination of (332), (111) and (331) facets (see Fig. 6(d)). The domination of the (332) facets on the surface and the high catalytic activity of the sample towards CO oxidation suggest the formation of the PdO(101) surface oxide, which was found by Westerström *et al.* to be the case when a Pd(553) crystal is exposed to pure oxygen. Upon further increase of the oxygen partial pressure a multilayer of PdO starts to grow on the surface with the [101] crystallographic direction parallel to the [111] and the [331] directions of the substrate (see Fig. 6(f)), while the catalytic activity remains mass transfer limited. When the reaction conditions are set to the initial CO rich environment the surface recovers directly to the (553) metallic state.

Acknowledgements

This work is done within the Röntgen-Ångström cluster "Catalysis on the atomic scale" financed by the Swedish research council (Project no. 349-2011-6491). The authors would like to acknowledge Deutsches Elektronen-Synchrotron (DESY) in Hamburg, Germany, where the experiments were performed.

References

1 I. Langmuir, *Trans. Faraday Soc.*, 1922, **17**, 621–654.
2 T. Engel and G. Ertl, Elementary Steps in the Catalytic Oxidation of Carbon Monoxide on Platinum Metals, in *Advances in Catalysis*, ed. D. D. Eley, H. Pines and P. B. Weez, Academic Press, 1979, vol. 28, pp. 1–78, DOI: 10.1016/S0360-0564(08)60133-9.
3 P. J. Berlowitz, C. H. F. Peden and D. W. Goodman, *J. Phys. Chem.*, 1988, **92**, 5213–5221.
4 J. Rodriguez and D. W. Goodman, *Surf. Sci. Rep.*, 1991, **14**, 1–107.
5 H. J. Freund, G. Meijer, M. Scheffler, R. Schlögl and M. Wolf, *Angew. Chem., Int. Ed.*, 2011, **50**, 10064–10094.
6 B. Lang, R. Joyner and G. Somorjai, *Surf. Sci.*, 1972, **30**, 440–453.
7 D. Castner and G. Somorjai, *Surf. Sci.*, 1979, **83**, 60–82.
8 G. Hoogers and D. King, *Surf. Sci.*, 1993, **286**, 306–316.
9 J. G. Wang, W. X. Li, M. Borg, J. Gustafson, A. Mikkelsen, T. M. Pedersen, E. Lundgren, J. Weissenrieder, J. Klikovits, M. Schmid, B. Hammer and J. N. Andersen, *Phys. Rev. Lett.*, 2005, **95**, 256102.
10 J. Gustafson, A. Resta, A. Mikkelsen, R. Westerström, J. N. Andersen, E. Lundgren, J. Weissenrieder, M. Schmid, P. Varga, N. Kasper, X. Torrelles, S. Ferrer, F. Mittendorfer and G. Kresse, *Phys. Rev. B: Condens. Matter Mater. Phys.*, 2006, **74**, 035401.
11 J. Gustafson, M. Shipilin, C. Zhang, A. Stierle, U. Hejral, U. Ruett, O. Gutowski, P.-A. Carlsson, M. Skoglundh and E. Lundgren, *Science*, 2014, **343**, 758–761.
12 M. Shipilin, U. Hejral, E. Lundgren, L. R. Merte, C. Zhang, A. Stierle, U. Ruett, O. Gutowski, M. Skoglundh, P.-a. Carlsson and J. Gustafson, *Surf. Sci.*, 2014, **630**, 229–235.
13 M. Shipilin, J. Gustafson, C. Zhang, L. R. Merte, A. Stierle, U. Hejral, U. Ruett, O. Gutowski, M. Skoglundh, P.-A. Carlsson and E. Lundgren, *J. Phys. Chem. C*, 2015, **119**, 15469–15476.
14 R. Westerström, J. Gustafson, A. Resta, A. Mikkelsen, J. N. Andersen, E. Lundgren, N. Seriani, F. Mittendorfer, M. Schmid, J. Klikovits, P. Varga, M. D. Ackermann, J. W. M. Frenken, N. Kasper and A. Stierle, *Phys. Rev. B: Condens. Matter Mater. Phys.*, 2007, **76**, 155410.
15 R. van Rijn, M. Ackermann, O. Balmes, T. Dufrane, A. Geluk, H. Gonzalez, H. Isern, E. de Kuyper, L. Petit, V. A. Sole, D. Wermeille, R. Felici and J. W. M. Frenken, *Rev. Sci. Instrum.*, 2010, **81**, 014101.
16 H. Reichert, V. Honkimäki, A. Snigirev, S. Engemann and H. Dosch, *Physica B*, 2003, **336**, 46–55.
17 H. Conrad, G. Ertl and J. Küppers, *Surf. Sci.*, 1978, **76**, 323–342.
18 A. Santra and D. Goodman, *Electrochim. Acta*, 2002, **47**, 3595–3609.
19 H. Gabasch, A. Knop-Gericke, R. Schlogl, M. Borasio, C. Weilach, G. Rupprechter, S. Penner, B. Jenewein, K. Hayek and B. Klotzer, *Phys. Chem. Chem. Phys.*, 2007, **9**, 533–540.
20 R. Toyoshima, M. Yoshida, Y. Monya, K. Suzuki, B. S. Mun, K. Amemiya, K. Mase and H. Kondoh, *J. Phys. Chem. Lett.*, 2012, **3**, 3182–3187.
21 S. Blomberg, M. Hoffmann, J. Gustafson, N. Martin, V. Fernandes, A. Borg, Z. Liu, R. Chang, S. Matera, K. Reuter and E. Lundgren, *Phys. Rev. Lett.*, 2013, **110**, 117601.
22 F. Zhang, T. Li, L. Pan, A. Asthagiri and J. F. Weaver, *Catal. Sci. Technol.*, 2014, **4**, 3826–3834.
23 G. Comsa, G. Mechtersheimer and B. Poelsema, *Surf. Sci.*, 1982, **119**, 159–171.
24 L. Niu, D. Koleske, D. Gaspar, S. King and S. Sibener, *Surf. Sci.*, 1996, **356**, 144–160.
25 T. P. Pearl and S. J. Sibener, *J. Chem. Phys.*, 2001, **115**, 1916–1927.
26 O. Balmes, G. Prevot, X. Torrelles, E. Lundgren and S. Ferrer, *J. Catal.*, 2014, **309**, 33–37.
27 H. Kondoh, R. Toyoshima, Y. Monya, M. Yoshida, K. Mase, K. Amemiya and B. S. Mun, *Catal. Today*, 2016, **260**, 14–20, DOI: 10.1016/j.cattod.2015.05.016.
28 E. Lundgren, G. Kresse, C. Klein, M. Borg, J. N. Andersen, M. De Santis, Y. Gauthier, C. Konvicka, M. Schmid and P. Varga, *Phys. Rev. Lett.*, 2002, **88**, 246103.
29 J. Jose, A. Hinojosa, H. H. Kan and J. F. Weaver, *J. Phys. Chem. C*, 2008, **112**, 8324–8331.
30 J. T. Hirvi, T.-J. J. Kinnunen, M. Suvanto, T. A. Pakkanen and J. K. Nørskov, *J. Chem. Phys.*, 2010, **133**, 084704, DOI: 10.1063/1.3464481.
31 G. Zheng and E. Altman, *Surf. Sci.*, 2000, **462**, 151–168.
32 J. Klikovits, E. Napetschnig, M. Schmid, N. Seriani, O. Dubay, G. Kresse and P. Varga, *Phys. Rev. B: Condens. Matter Mater. Phys.*, 2007, **76**, 045405.
33 H. H. Kan and J. F. Weaver, *Surf. Sci.*, 2008, **602**, L53–L57.
34 N. M. Martin, M. V. den Bossche, H. Grönbeck, C. Hakanoglu, J. Gustafson, S. Blomberg, M. A. Arman, A. Antony, R. Rai, A. Asthagiri, J. F. Weaver and E. Lundgren, *J. Phys. Chem. C*, 2013, **117**, 13510–13519.

35 J. Xu and J. T. Yates, *J. Chem. Phys.*, 1993, **99**, 725–732.
36 T. Zambelli, J. Wintterlin, J. Trost and G. Ertl, *Science*, 1996, **273**, 1688–1690.
37 S. Dahl, A. Logadottir, R. C. Egeberg, J. H. Larsen, I. Chorkendorff, E. Törnqvist and J. K. Nørskov, *Phys. Rev. Lett.*, 1999, **83**, 1814–1817.
38 T. Zubkov, G. A. Morgan Jr., J. T. Yates Jr., O. Kühlert, M. Lisowski, R. Schillinger, D. Fick and H. J. Jänsch, *Surf. Sci.*, 2003, **526**, 57–71, DOI: 10.1016/S0039-6028(02)02655-9.
39 R. T. Vang, K. Honkala, S. Dahl, E. K. Vestergaard, J. Schnadt, E. Laegsgaard, B. S. Clausen, J. K. Norskov and F. Besenbacher, *Nat. Mater.*, 2005, **4**, 160–162.
40 B. Tränkenschuh, N. Fritsche, T. Fuhrmann, C. Papp, J. F. Zhu, R. Denecke and H.-P. Steinrück, *J. Chem. Phys.*, 2006, **124**, 74712.
41 R. Streber, C. Papp, M. P. A. Lorenz, A. Bayer, R. Denecke and H.-P. Steinrück, *Angew. Chem., Int. Ed.*, 2009, **48**, 9743–9746.
42 R. Streber, C. Papp, M. P. A. Lorenz, A. Bayer, S. Wickert, M. Schöppke, R. Denecke and H.-P. Steinrück, *J. Phys.: Condens. Matter*, 2009, **21**, 134018.
43 L. Jacobse, A. den Dunnen and L. B. F. Juurlink, *J. Chem. Phys.*, 2015, **143**, 014703.
44 C. Popa, T. Zhu, I. Tranca, P. Kaghazchi, T. Jacob and E. J. M. Hensen, *Phys. Chem. Chem. Phys.*, 2015, **17**, 2268–2273.